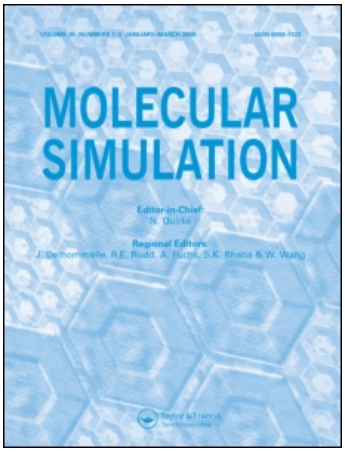

Molecular Simulation
Publication details, including instructions for authors and subscription information:
http://www.informaworld.com/smpp/title~content=t713644482

Continuum Percolation of *2D* and 3*D* Simple Fluids

D. M. Heyes[a]; J. R. Melrose[a]
[a] Department of Chemistry, Royal Holloway and Bedford New College, University of London, Surrey, UK

To cite this Article Heyes, D. M. and Melrose, J. R.(1990) 'Continuum Percolation of *2D* and 3*D* Simple Fluids', Molecular Simulation, 5: 5, 329 — 343
To link to this Article: DOI: 10.1080/08927029008022418
URL: http://dx.doi.org/10.1080/08927029008022418

Molecular Simulation, 1990, Vol. 5, pp. 329–343
Reprints available directly from the publisher
Photocopying permitted by license only

CONTINUUM PERCOLATION OF 2*D* AND 3*D* SIMPLE FLUIDS

D.M. HEYES and J.R. MELROSE

Department of Chemistry, Royal Holloway and Bedford New College, University of London, Egham, Surrey TW20 0EX, UK

(*Received January 1990, accepted February 1990*)

We use Monte Carlo and Molecular Dynamics computer simulations to investigate the percolation threshold, ρ_p, of d-dimensional Lennard-Jones *LJ*, and square-well fluids. We find that when the range of the potential well is small compared to the hard-core diameter (in the so-called 'hard-core' limit), an attractive well decreases ρ_p below the high temperature limiting value. In contrast, a hard shoulder potential produces the opposite trend. We investigate the structure of the 2*D* percolating clusters, in particular, the effects of periodic boundaries. We examine the shapes of the 3*D* clusters at the percolation threshold, resolved as a function of the number of particles in a cluster, s. The asphericity parameter, A_3, describing the instantaneous shape of the cluster decays slowly from unity, typically only achieving ~ 0.3 by $s \sim 100$, close to the estimated universal value of 0.312.

We focus especially on the relationship between long and short range structural order as probed by the coordination numbers of the molecules. We also use a cluster-resolution of the co-ordination number to indicate the degree of branching in the clusters, and how it is influenced by the number of atoms in the cluster and temperature for the different potentials. We look forward to future directions for simulation in investigating physical properties in the vicinity of the percolation threshold.

KEY WORDS: Percolation, coordination numbers, fluids.

1. INTRODUCTION

Long-range connectivity, or **percolation** has consequences in many branches of chemical physics, for example in determining the rheological properties of colloidal dispersions [1], the porosity of rocks [2] and the conductivity of random particle assemblies [3], for example. Some major advances in the area of continuum percolation (where the 'connecting' units are not confined to lattice sites, as in the early pioneering work) have been made in the 1980's [4–12]. Continuum percolation is a much more realistic representation of many physical systems because, as the particles are not confined to lattice points, the local structure and hence the physical properties derived from it are modelled more realistically. (Although the same universality of the exponents for lattice and continuum exponents is expected to hold.) In this looser arrangement, with variable co-ordination number, pairs of particles are considered to be directly connected if their two centres lie within an arbitrary distance, σ_s, which need not be formally related to the range of the pair potential [2].

Our concern here is to focus in more detail on the effect of intermolecular interactions and temperature on the percolation threshold and distributions of coordination numbers within the clusters. In this study we consider molecules that interact through continuous and discontinuous pair potentials in both 2*D* and 3*D*. In the latter class,

the model molecules interact here via a square-shaped pair potential with a potential minimum or shoulder $\sim k_B T$ [7]. The particles interact via the square-well or square-shoulder pair potential,

$$\begin{aligned} \phi(r) &= \infty, \quad r \leqslant \sigma, \\ &= -\varepsilon, \quad \sigma < r \leqslant \lambda\sigma, \\ &= 0, \quad r > \lambda\sigma, \end{aligned} \tag{1}$$

The hard-core diameter of the particles is σ. For attractive wells, $\varepsilon = 1$, and for repulsive shoulder particles, $\varepsilon = -1$. We use,

$$\sigma_s = \lambda\sigma, \tag{2}$$

The different regimes of the potential are separated by sharp boundaries in the pair separation, r. The connectivity distance, σ_s equals the range of the potential-well. We also consider the Lennard-Jones potential, which changes from repulsive to attractive **continuously** as r increases,

$$\phi(r) = 4\varepsilon((\sigma/r)^{12} - (\sigma/r)^6). \tag{3}$$

We conclude with a discussion of the potential of molecular simulation to determine the dynamical properties of fluids in the vicinity of the percolation cluster.

2. THEORY

One method of determining clusters is the same as that reported previously [13, 15]. For the square-well potentials, the disks ($2D$) or spheres ($3D$) have a central hard core of diameter, σ and an outer shell of diameter, $\lambda\sigma$. There is a flat pair potential of magnitude, ε, in the outer annulus. The particles are partially permeable (or 'soft-shells') of diameter $\sigma_s = \lambda\sigma$ centred on those of the hard-cores. Particles are connected if their soft-shells overlap. Percolation occurs when a connected cluster spans the infinite replica system considered in the simulation. As σ_s diminishes, the repulsive core and attractive outer region of the particle influences the nature of the clusters formed out of the soft-shells and thereby affects the percolation characteristics. As $\sigma_s/\sigma \to 1$ the overlap of the soft-shells becomes strongly influenced by the excluded volume effects of the impenetrable core. This we term the soft- core to hard- core transition.

We evaluated the function, P, the fraction of configurations (time steps) generated by the computer that manifested at least one percolating cluster (PC). The percolation threshold in the thermodynamic limit (*i.e.*, the number of particles in the simulation cell, $N \to \infty$), ρ_p, is best estimated for finite N when $P = 0.5$, because it shows the smallest system-size (*i.e.*, N) dependence. The reason for the 'pre-percolation' that occurs at lower densities, $\rho < \rho_p$, for finite periodic systems is explained here.

The distribution of different sized clusters is characterised by the cluster number distribution function, n_s, the time- average number of clusters containing s particles, N_s divided by N *i.e.*, $n_s = N_s/N$ [5]. At the percolation threshold,

$$n_s(\rho_p) \sim s^{-\tau}, \; s \to \infty. \tag{4}$$

For finite periodic systems there is an upper bound on s, *i.e.*, $1 \leqslant s \leqslant N$, resulting in distortions from Equation (4) for $s \to N$.

There is a similar scaling law for the length-scale of a cluster. At least, for the small clusters generated by molecular simulation, this is no unique definition for this quantity. One could use the maximum separation of any two particles as a measure of the length-scale of a cluster. However, it is more usual to use the radius of gyration as a measure of the length-scale. But even with this quantity there are a number of slightly inconsistent formulae to be found in the literature. We show below that these can give noticeably different results for the radius of gyration for small cluster sizes. We have,

$$R_g = \left\langle \sum_i^s (\mathbf{R}_i - \mathbf{R}_{cm})^2/s \right\rangle^{1/2},$$
$$= \left\langle \frac{1}{2} \sum_i^{s-1} \sum_{j \neq i}^{s} \mathbf{R}_{ij}^2/s^2 \right\rangle^{1/2}. \quad (5)$$

where the centre of mass position, $\mathbf{R}_{cm} = \sum_i^s \mathbf{R}_i/s$. In the limit of $R_g \to \infty$,

$$R_g \to \left\langle \frac{1}{2} \sum_i^{s-1} \sum_{j \neq i}^{s} \mathbf{R}_{ij}^2/s(s-1) \right\rangle^{1/2}. \quad (6)$$

where $\mathbf{R}_{ij}$ is the vector separation between particles i and j. We have used this latter expression in our earlier reports of continuum percolation [13–15]. At the percolation threshold, the radius of gyration, R_g, provides a route to the fractal dimension, D_f of the non-percolating clusters. The scaling relationship here is $R_g \sim s^{1/D_f}$ as $s \to \infty$.

The pair radial distribution function, $g(r)$ and pair connectedness function, $p(r)$, for pair separations, r, are probes of the local structure in the whole fluid and within the clusters, respectively [3]. In $3D$,

$$g(r) = n(r)/(4\pi r^2 \rho \delta r). \quad (7)$$

where δr is the radial increment for $n(r)$; $n(r)$ is the number of particles found on average within $r - \delta r/2 \leqslant r \leqslant r + \delta r/2$.

If P_∞ is the fraction of molecules in the percolating cluster, PC, then at ρ_p,

$$p(r) = n(r)' P_\infty/(4\pi r^2 \rho \delta r). \quad (8)$$

where $n(r)'$ is the number of particles found on average within $r - \delta r/2 \leqslant r \leqslant r + \delta r/2$ within the same cluster. (All clusters are used for this, not just the PC). As $r \to \infty$ then $p(r) \to P_\infty^2$. Therefore, the $p(r)$ look similar to the $g(r)$ but attain a lower limiting value when the pair separation becomes comparable to the size of the periodic cell. In the limit, $r \to \infty$, in $3D$ we have $p(r) \sim r^{D_f - 3}$. In practice, we found that D_f is obtained more accurately from the function,

$$m(r) = \int_0^r n(r')dr', \quad (9)$$

which has the limiting value $m(r) \sim r^{D_f}$ for large $r \to \infty$.

We measure the instantaneous shape of the clusters using the method of Bishop and co-workers [16,17]. The shape of each cluster is determined from the tensor components of the radius of gyration. The trace of this is equal to R_g^2 and the eigenvalues, λ_i, are the components of R_g^2 along the principal orthogonal axes.
In dimension, d, the asphericity, A_d, of the cluster is measured by [17],

$$A_d = \frac{\sum_{i>j}^{d} \langle (\lambda_i - \lambda_j)^2 \rangle}{(d-1) \langle (\sum_{i=1}^{d} \lambda_i)^2 \rangle}, \tag{10}$$

If the cluster is highly symmetric, roughly spherical, then $A_d \to 0$, whereas if it is rod-shaped, then $A_d = 1$.

3. SIMULATION DETAILS

The Metropolis *MC* calculations were performed on cubic unit cells of volume V containing $N = 256$ and $N = 500$ hard-core particles. The simulations were for typically ~ 8000 attempted moves per particle for $N = 256$ and for ~ 4000 attempted moves per particle for $N = 500$. The maximum displacement distance per particle was periodically adjusted in order achieve a move acceptance fraction of 0.5. We employ the following reduced units throughout, i.e., , σ for distance, $k_B T/\varepsilon \to T$, and number density, $\rho = N\sigma^3/V$.

We also consider the results of Molecular Dynamics *MD* simulations on *2D* Lennard-Jones fluids [14]. In this case the connectivity distance, σ_s is in *LJ* units.

4. RESULTS AND DISCUSSION

We find that it is instructive to distinguish those states where the hard-core of the molecule forms a substantial fraction of the volume of the square-well (the so-called 'hard-core' limit) from those states in which the hard-core is insignificant in volume compared with that of the square-well. In this latter, 'soft-core' limit the particles are effectively interpenetrable.

In the hard-core limit (*e.g.*, $\sigma_s \leqslant \sim 1.7\sigma$), in the attractive well fluid phase, the value of ρ_p decreases with decrease in temperature from $T = 10 \to 0.5$, the range considered here. The ρ_p manifest a curvature to **lower** density as T decreases. For example, using $\lambda = 1.1$, $\rho_p = 0.55,0.53$ and 0.42 for $T = 10,4$ and 1, respectively. Towards the soft-core limit, the $\sigma_s \geqslant 2.0$ lines increasingly show a ρ_p that shift towards **higher** density as temperature decreases. Taking $\lambda = 2.5$, and $T = 10,4,1$ we have $\rho_p = 0.039,0.035$ and 0.085, respectively. These trends are present in both *2D* and *3D*, and were originally observed by Bug *et al.* for *2D* square-wells [13]. As temperature decreases the attractive square wells cause the network to become more chain-like in the hard-core limit. Neighbours are attracted within the well-range in order to reduce the energy of the system. Therefore a lower density of particles is required to induce percolation at constant, σ_s(*i.e.*, ρ_p decreases). In the soft-core limit the effect of a decrease in temperature is to cause an enhanced 'bunching' of particles into small clusters leading to a reduction in long-range connectivity and an increase therefore in ρ_p. In the hard-core limit this bunching cannot occur, as the hard-core limits the extent of overlap.

The attractive *SW* and *LJ* fluids both show this cross-over between 'bunching' and 'chaining'-dominated regimes in percolation behaviour. At the boundary between these two regimes, at $\sigma_s \sim 2.0\sigma$, the percolating cluster shows both chaining **and** bunching, as revealed in Figure 1 for a *2D LJ* fluid. At this value of σ_s there is

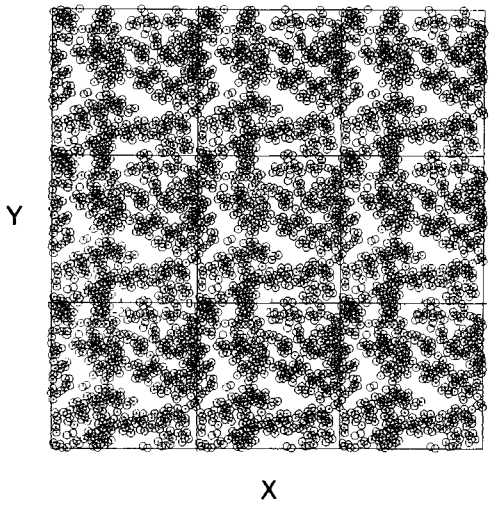

Figure 1 Pictorial illustration of non-percolating and percolating clusters in two-dimensional *MD* cells for the *LJ* fluid at $\rho_p = 0.307$, $T = 0.6$, $\sigma_s = 2.0$, $N = 450$. The large circles mark out the soft-cores of the molecules. Those dotted are part of the percolating cluster.

consequently a weak dependence of the percolation threshold on temperature. Figure 2 shows that percolation at ρ below ρ_p **can** take place in these finite-periodic systems. The percolating clusters formed generally lie parallel to the sidelengths of the cell, this forming the shortest distance between a particle and its image (the necessary conditions for percolation of a single cluster). In Figure 3 we show pictures of the fluid structure in the hard-core limit at three times separated by 1 *LJ* time unit. These pictures show the particles that belong to a percolating cluster. These pictures illu-

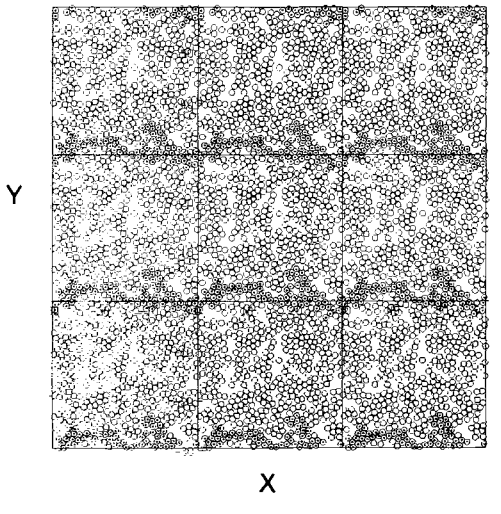

Figure 2 As for Figure 1, except the state point is at a density which is $\sim 15\%$ below ρ_p. $\rho = 0.519$, $T = 1$, $\lambda = 1.2$, $S = 29.5\sigma$, where S is the simulation cell sidelength.

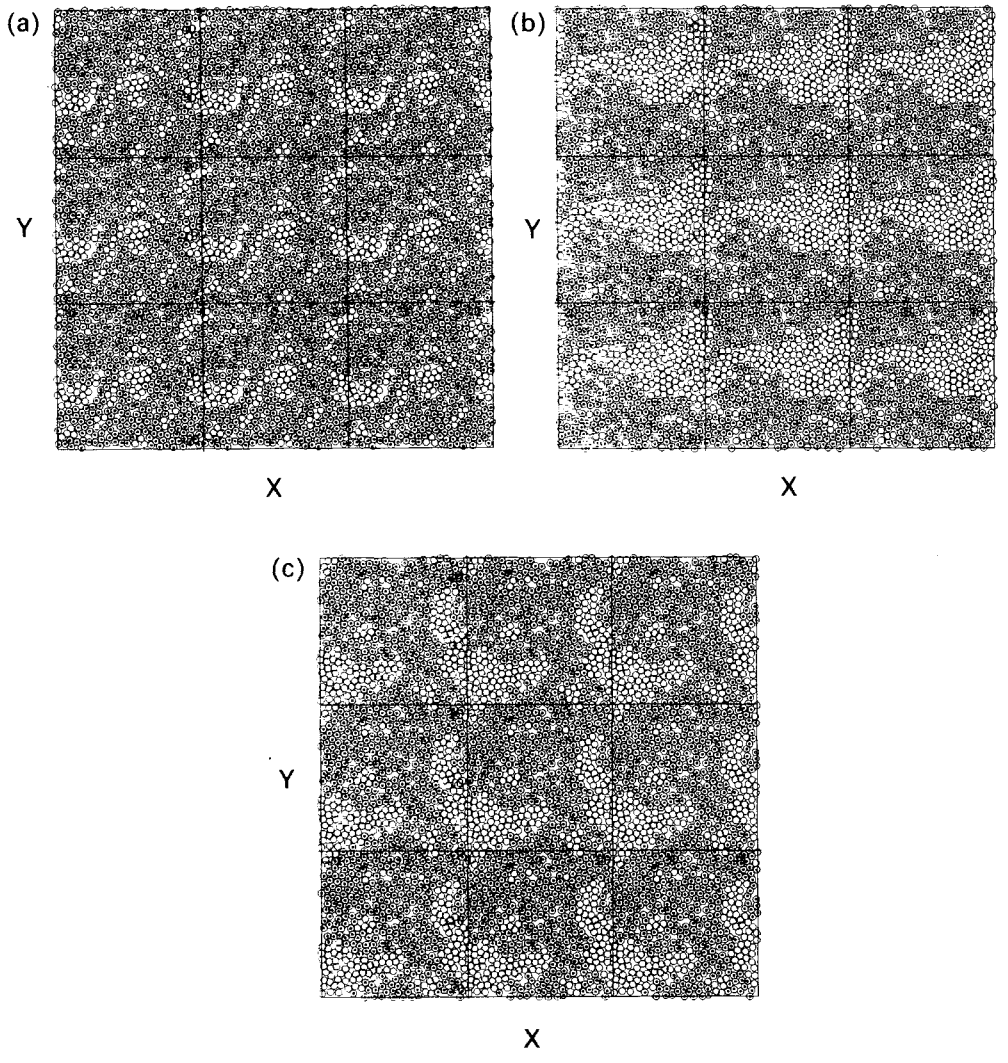

Figure 3 The time dependence of the percolating configurations for the *LJ* state: $\rho_p = 0.987$, $T = 10$, $\lambda = 1.0$, $S = 21.4$. Figures (a), (b) and (c) are in chronological order, separated by $1LJ$ time unit.

strate that, on a molecular timescale, the form of the percolating clusters changes dramatically.

In contrast, the repulsive 'square shoulder', *SS*, fluids have an increasing ρ_p as temperature decreases, for **all** λ values. For example, for $\lambda = 1.05$, and $T = 10$,2 and 0.5, we have $\rho_p = 0.773$,0.835 and 0.989 for $N = 500$ particle *MC* systems. As there is no liquid-gas coexistence region produced by the *SS* potential, we do not observe any anomalous trends in ρ_p as we vary σ_s or equivalently λ, at $T \sim 1$. This behaviour of the *SS* fluids is caused as particles depart from the region of radius λ about each particle as the temperature is lowered. Therefore local connectivity is reduced and a higher density is required to induce percolation.

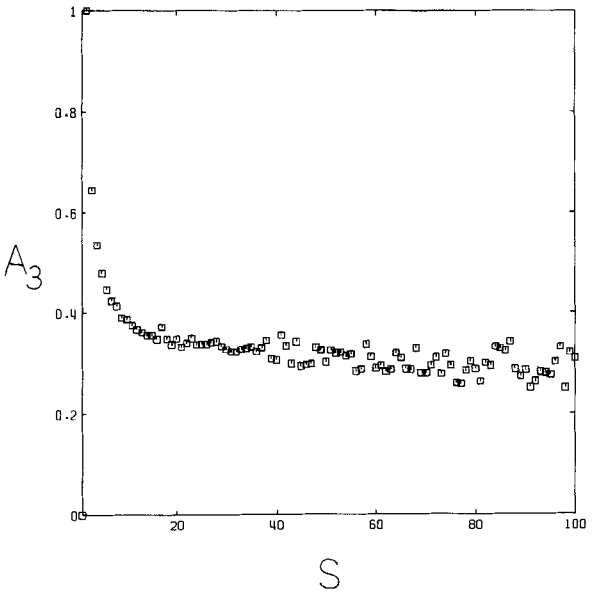

Figure 4 The asphericity parameter, A_3 from Equation (6), for a $3D$ attractive square-well state point, $\rho_p = 0.7391$, $T = 10$, $\lambda = 1.05$, $N = 256$.

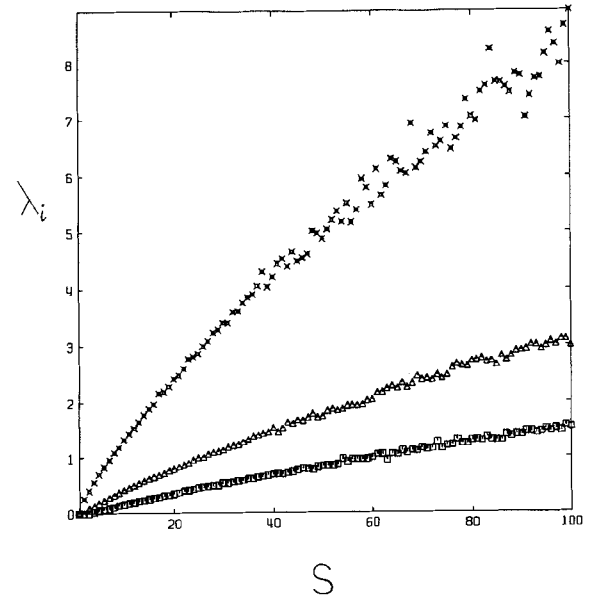

Figure 5 The λ_i, the components of R_g^2, used in Equation (10) along the principal orthogonal axes, for the state point of Figure 4.

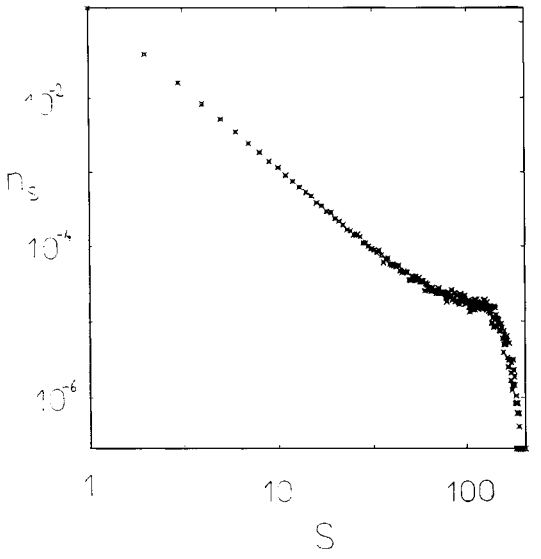

Figure 6 The cluster number distribution function defined in Equation (4) for the attractive square well state point, $T = 10$, $\rho_\rho = 0.739$, $\lambda = 1.05$, $N = 256$. The measured exponent, $\rho' = 2.18 \pm 0.04$.

In Figure 4 we show the parameter, A_3 for representative state points at the percolation threshold. We note that for the non-percolating clusters A_3 decreases from 1 at $s = 2$ to $A_3 \simeq 0.5$ at $s = 5$. The overall trend above the statistical fluctuations reveals that the subsequent decrease is slow, *i.e.*, $A_3 \simeq 0.3$ for $s \sim 200$, statistically the same as the universal value for the percolating cluster, $A_3 = 0.312$ [16,17]. In Figure 5 we show the corresponding λ_i used in Equation (7).

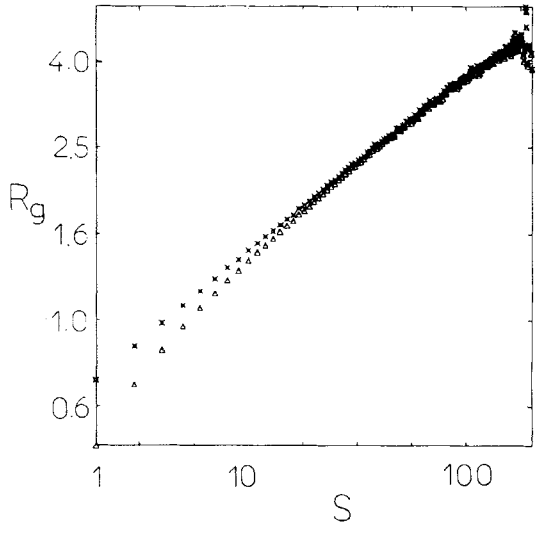

Figure 7 A comparison between Equations (5) (△) and (6) (×) for $R_g^2(s)$, the dimensions of the cluster of s particles at the percolation threshold (only nonpercolating clusters are considered here.) State point: $T = 10$, $\rho_\rho = 0.739$, $\lambda = 1.05$, $N = 256$.

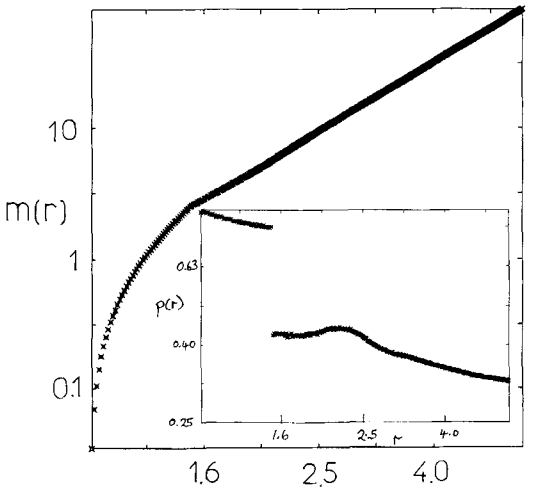

Figure 8 The radial integrated number, $m(r)$ and $p(r)$, from Equations (8) and (9), respectively, as the insert, for the 3D *SQW* state point, $\lambda = 1.5$, $\rho = 0.1733$, $T = 10$, $N = 256$. $D_f = 2.55 \pm 0.08$, for both figures.

The cluster number distribution function, $n_s(s)$ has the exponent, $\tau = 2.2$ on a $3D$ lattice [18]. We find that in the fluid phase, the measured exponent, τ', is less than this value in the (high-density) hard-core limit $\tau = 2.05 \pm 0.10$, see for example the example given in Figure 6. The value of τ' decreases to an even smaller value in the (low density) soft-core limit $\sim 1.7 \pm 0.1$. (We use the notation τ' rather than τ here because τ is defined as the exponent of n_s in the asymptotic limit of $N \to \infty$). We

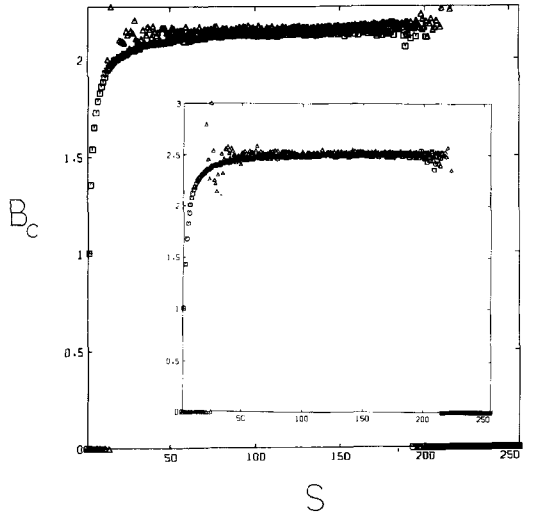

Figure 9 The cluster dependent coordination number per particle, $B_c(s)$, for non-percolating clusters, □, and percolating cluster △. Attractive square wells are considered. State for the main figure: $T = 10$, $\rho_p = 0.739$, $\lambda = 1.05$, $N = 256$. The insert is the soft-core state, $T = 10$, $\rho_p = 0.173$, $\lambda = 1.5$, $N = 256$.

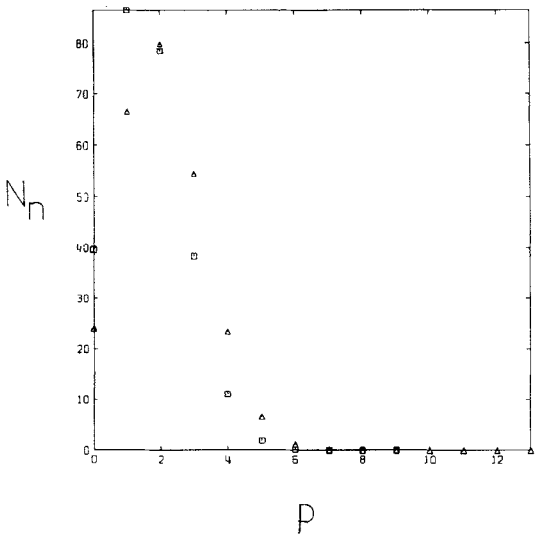

Figure 10 The average number of particles with p directly connected neighbours, $N_n(p)$ for the state: $T = 10$, $\rho_p = 0.739$, $\lambda = 1.05$, $N = 256$ (□) and $T = 10$, $r_p = 0.173$, $\lambda = 1.5$, $N = 256$ (△).

believe that the low values to be finite size effects. The periodic boundary conditions enhance the number of large clusters (before the sharp cut-off at $s = N$). This is especially extreme in the soft-core limit as $\sigma_s/L \to \infty$, where L is the length of the simulation cell. For much larger systems (at present beyond the scope of molecular simulation) the evaluated τ' should increase to the universal value, that is $\tau' \to \tau$.

The non-percolating and percolating clusters formed from non-interacting particles on a lattice at ρ_p manifest the same fractal dimension, D_f. For non-interacting particles, percolation theory gives $D_f = d - \beta/\nu$, where d is the dimension of the space and β and ν are the universal percolation exponents. In $2D$, $\beta = 0.139$ and $\nu = 1.333$ [18], $D_f = 1.90$. Also in $3D$, $\beta = 0.4$ and $\nu = 0.9$ [18], $D_f = 2.5$. The two-estimates for the size of the cluster, R_g, give quite different values for small s. The rigorous definition of R_g from Equation (5) gives a lower value than that from Equation (6). The usual prescription used from Equation (6) follows the high s slope more closely at low s values. In Figure 7 we show the $R_s(s)$ for a high temperature hard-core attractive square well state. We therefore prove that, for the small system sizes typically employed in molecular simulation, Equation (6) gives a better estimate for the fractal dimension of the large clusters. Equation (9) gives a value of 2.7 ± 0.1 for D_f in $3D$, which bearing in mind the small size of the system, is in quite reasonable agreement with the universal value of 2.5. In $2D$ we find that $D_f = 1.9 \pm 0.1$, in agreement with the universal value of 1.9. Figure 8 presents a typical example of $m(r)$ leading to an estimate of D_f.

We make a resolution of the average co-ordination number of the particles within clusters of size, s, denoted $B_c(s)$. This extends the ideas of earlier work on B_c, the average coordination number of all the particles in the system [4,6]. In the high-temperature soft-core limit, $B_c = 2.9$, and in the hard-core limit, $B_c = 1.5$. Our results are consistent with these bounds. For example at a state close to the soft-core

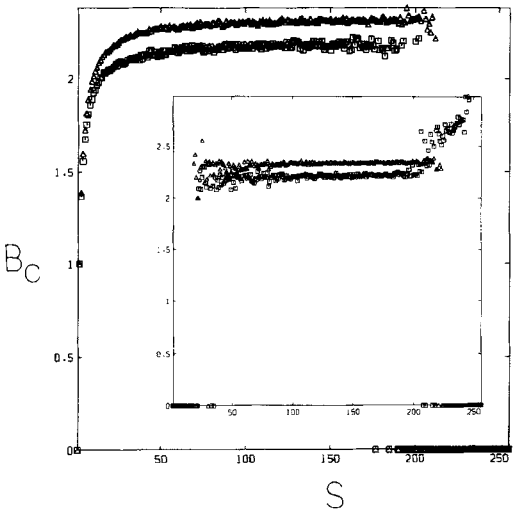

Figure 11 The cluster dependent coordination number per particle, $B_c(s)$, for non-percolating clusters, (main figure) and percolating clusters (insert). Attractive square wells are considered. States considered: $T = 10$, $\rho_p = 0.553$, $\lambda = 1.1$, $N = 256$ (□). $T = 1$, $\rho_p = 0.417$, $\lambda = 1.1$, $N = 256$ (△).

limit, $\rho_p = 0.0392$, $T = 10$, $N = 256$, $\lambda = 2.5$ we have $B_c = 2.55$. Similarly, approaching the hard-core limit, we have for $\rho_p = 0.7391$, $T = 10$, $N = 256$, $\lambda = 1.05$ we have $B_c = 1.61$. We further resolve, $B_c(s)$, into contributions from nonpercolating and percolating clusters. A typical example of these functions is presented in Figure 9. One striking feature of $B_c(s)$ is the wide range of coordination numbers, from $s = 2$ to $s = N$, the upper limit of the simulation. The coordination number increases with s. In the large s limit the nonpercolating and percolating cluster $B_s(s)$ tend to the same value. However, for the small systems and clusters accessed by molecular simulation we note that as, s, decreases the average coordination number for the percolating clusters is larger than that of the nonpercolating clusters at the same s. This is because when an isolated cluster transforms into a percolating cluster by molecular rearrangement, it forms new bonds to 'itself' across the periodic boundaries. The average coordination number then manifests a sudden increase. The difference between, $B_c(s)$, for nonpercolating and percolating clusters increases as s diminishes because the average number of 'extra' bonds per particle formed on percolation becomes a larger percentage of the whole. We also note that, $B_c(2) = 1$ and there is a slow approach to the large cluster value. Obviously, $B_c(s \to \infty) > B_c$, as the smaller clusters have a lower cooordination number than the average. We note, for example, that at $\rho_p = 0.7391$, $T = 10$, $N = 256$, $\lambda = 1.05$ we have $B_c(s \to \infty) = 2.14$ and $B_c = 1.61$. Also for, $\rho_p = 0.5527$, $T = 10$, $N = 256$, $\lambda = 1.1$ we have $B_c(s \to \infty) = 2.20$ and $B_c = 1.71$; and for $\rho_p = 0.1733$, $T = 10$, $N = 256$, $\lambda = 1.5$ we have $B_c(s \to \infty) = 2.53$ and $B_c = 2.05$.

An alternative representation of the local connectivity of the clusters is to resolve the number of particles with p bonds to other particles, $N_n(p)$ [6]. In contrast to $B_c(s)$, this function shows the extremes of coordination generated during the simulation. The example of Figure 10 shows the complementary information given by B_c and $N_c(p)$. B_c gives the average number of bonds to neighbours, whereas $N_n(p)$ gives the

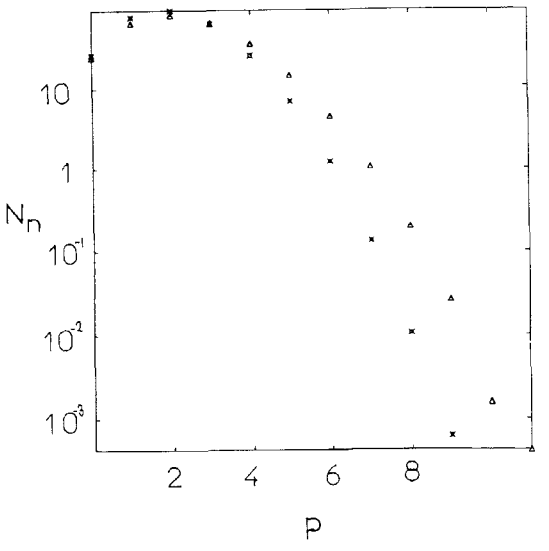

Figure 12 $N_n(p)$ for $\rho_p = 0.173$, $T = 10$, $\lambda = 1.5$, ×, and $\rho_p = 0.1491$, $T = 2$, $\lambda = 1.5$, △.

distribution of bonds per particle. The peak in $N_n(p)$ occurs at $p = 1$ and 2 in the hard-core and soft-core states considered, respectively.

We now consider, *for the first time*, how attractive interactions affect $B_c(s)$ and $N_n(p)$. Figure 11 shows the effect of temperature on $B_c(s)$. As temperature decreases close to the hard-core limit, $B_c(s \to \infty)$ increases from $T = 10$ to $T = 1$ using $\lambda = 1.1$ we get enhanced 'chaining' and a consequent decrease in ρ_p from

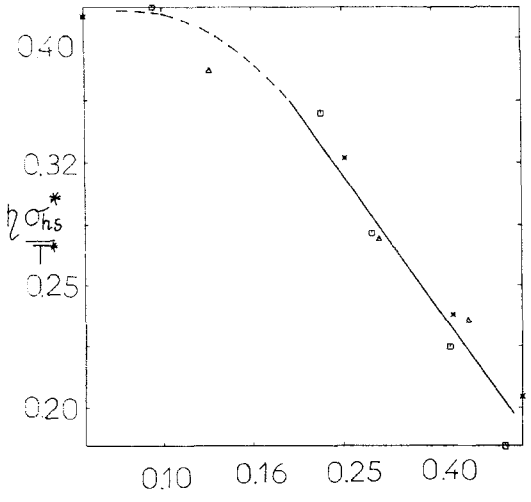

Figure 13 Test of the scaling relationship, $\eta \sim \varepsilon^{-k}$. The viscosities are reduced by the effective hard sphere diameter and the kinetic energy is scaled out. In the resonably linear regime we find, $k = 0.5 \pm 0.1$. Key: $T = 1.86$, ×, $T = 2.5$, △ and $T = 6.0$, □

$0.553 \rightarrow 0.417$. The accompanying $B_c(s \rightarrow \infty)$ increase from $2.20 \rightarrow 2.33$, and B_c from $1.71 \rightarrow 1.85$. The $N_n(p)$ in Figure 12 also reflects this effect. We note that a decrease in temperature at this value of λ enables the fluid to produce a greater number of large coordinated particles, up to 10.

A percolation transition is an accepted model of the sol/gel transition [19]. The shear viscosity η diverges to a singularity as the 'distance' from the percolation threshold, $\varepsilon = (\rho - \rho_p)/\rho_p \rightarrow 0$. Additionally, the infinite frequency shear modulus, G_∞ increases above the gel point. Both η and G_∞ approach the percolation threshold as a power law, $\sim |\varepsilon|^k$. This change in behaviour on crossing the percolation threshold is subject to there being a divergence in the average structural relaxation time at this density [20]. For simple fluids, where (a) the interactions are much weaker than those leading to gelation and (b) for continuous potentials there is no clearly dominating intermolecular pair separation governing the dynamics, which enable us to ascribe a unique value of σ_s and hence ρ_p for dynamical behaviour, we encounter a much weaker transition in dynamical behaviour in dynamical properties at ρ_p. In contrast to gelation, there is no divergence in the structural relaxation time at ρ_p for the molecular fluids considered here. In Figure 13 we analyse the *LJ* shear viscosity data of [21] to test for this scaling. We map the viscosities of three isotherms onto a single curve by reducing the viscosity and density by the effective hard-sphere diameter [22] and scaling out the trivial (low density) kinetic, $T^{1/2}$, temperature dependence. In a previous publication in this series, we established that there is a dramatic change in these physical properties at an equivalent effective hard-sphere critical volume fraction, $\phi_p = 0.25$ [23]. Figure 13 demonstrates that there is a power law regime. Also the data from the three isotherms collapse onto the same line. (This latter observation is perhaps not so surprising as the effectiveness of an equivalent hard-sphere fluid reduction of *LJ* viscosities has already been demonstrated [22].) The exponent we obtain, $k = 0.5 \pm 0.1$ is somewhat lower than a value recently quoted for condensation polymerisation $= 0.8$ [19].

4. CONCLUSIONS

In this work we have continued and reviewed our investigations of continuum percolation of molecular fluids. The percolation threshold of simple fluids in 2 and 3 dimensions shows a strong dependence on the underlying thermodynamic state. Attractive potentials at long range show a decrease in the value of the percolation threshold as temperature falls, in all but the most dilute state points. The reverse behaviour is manifest by repulsive 'shoulder' potentials. The coordination numbers of the clusters are resolved and compared with the system averages. The average coordination number of the clusters increases to a plateau value for clusters greater than approximately 100 particles in size.

Molecular simulation has proved itself effective in routinely determining the percolation thresholds of simple fluids with three digit accuracy. Bearing in mind finite size effects, we conclude that molecular simulation generates static percolation exponents that are reasonably close to the universal values. However, for the same computational effort lattice simulations can model larger systems than molecular simulation. As finite N effects are the main source of uncertainty in the percolation exponents, we conclude that the exponents are obtained more effectively using lattice simulations.

At present no formal relationship is known between static percolation aspects such as ρ_p, D_f, τ etc and the dynamical exponents. Therefore, the characterisation of the rheology (*e.g.*, dynamic moduli and viscosity) and conductivity of simple fluids (and closely related colloidal suspensions) in the vicinity of the percolation threshold is a major challenge for simulation. We argue that for all, except perhaps conductivity, the lattice approach is a serious oversimplification and could distort the essential physics of the experimental (continuum) systems. For example, the elastic moduli of springs on a lattice ignores any time-scale for relaxation and fixes the springs into an arrangement which could be metastable. Viscosity approaching the sol to gel transition is an even better example of a property for which it is hard to imagine a lattice simulation model. These are topics that we perceive as major challenges of Molecular (and Brownian) Dynamics.

Acknowledgements

D.M.H. gratefully thanks *The Royal Society* for the award of a *Royal Society 1983 University Research Fellowship*. J.R.M. thanks CASTROL Ltd. for the award of a research fellowship. The S.E.R.C. is thanked for the award of computer time on the CRAY-XMP at the University of London Computer Centre, and the RHBNC Computer Centre for use of their computing facilities. We express our thanks to Prof. J.G. Powles (University of Kent) for helpful discussions.

References

[1] C. Cametti, P. Codastefano, A. Di Biasio, P. Tartaglia and S.H. Chen, "Dynamic scaling of dielectric relaxation in sodium di(2-ethylhexyl)sulfosuccinate-water-decane microemulsions near the percolation threshold", *Phys. Rev. A*, **40**, 1962 (1989).
[2] I. Balberg, "Excluded-volume explanation of Archie's Law", *Phys. Rev. B*, **33**, 3618 (1986).
[3] F. Bruni, G. Vareri and A.C. Leopold, "Critical exponents of protonic percolation in maize seeds", *Phys. Rev. A*, **40**, 2803 (1989).
[4] I. Balberg, "Recent developments in continuum percolation", *Phil. Mag. B*, **56**, 991 (1987); J. Janzen, "On the critical conductive filler loading in antistatic composites", *J. Appl. Phys.*, **46**, 966 (1975).
[5] I. Balberg, "Nonuniversal behavior of the cluster properties of continuum systems", *Phys. Rev. B*, **37**, 2391 (1988).
[6] I. Balberg and N. Binenbaum, "Invariant properties of the percolation thresholds in the soft-core-hard-core transition", *Phys, Rev. A*, **35**, 5174 (1987).
[7] A.I.R. Bug, S.A. Safran, G.S. Grest and I. Webman, *Phys. Rev. Lett.*, **55**, 1896 (1985).
[8] N.A. Seaton and E.D. Glandt, "Aggregation and percolation in a system of adhesive spheres", *J. Chem. Phys.*, **86**, 4668 (1987).
[9] Y.C. Chiew and Y.H. Wang, "Percolation and connectivity of the attractive square-well fluid: Monte Carlo simulation study", *J. Chem. Phys.*, **89**, 6385 (1988).
[10] S.C. Netemeyer and E.D. Glandt, "Percolation behavior of the square-well fluid", *J. Chem. Phys.*, **85**, 6054 (1986).
[11] E.M. Sevick, P.A. Monson and J.M. Ottino, "Monte Carlo calculations of cluster statistics in continuum models of composite morphology", *J. Chem. Soc.*, **88**, 1198 (1988).
[12] S.B. Lee and S. Torquato, "Pair connectedness and the mean cluster size for continuum-percolation models: Computer-simulation results", *J. Chem. Phys.*, **89**, 6427 (1988).
[13] D.M. Heyes and J.R. Melrose, "Continuum percolation of 2*D* Lennard-Jones and square-well phases", *Mol. Phys.*, **68**, 359 (1989).
[14] N. Cooper, A. Tedder, D.M. Heyes and J.R. Melrose, "Percolation cluster statistics of 2*D* Lennard-Jones phases", *J. Phys.: Condens. Matter*, **1**, 6217 (1989).
[15] D.M. Heyes and J.R. Melrose, "Percolation cluster statistics of Lennard-Jones fluids", *Mol. Phys.*, **66**, 1057 (1989).
[16] J. Rudnick and G. Gaspari, "The shapes of random walks", *Science*, **237**, 384, (1987).

[17] M. Bishop and C.J. Saltiel, "Polymer shapes in two, four and five dimensions", *J. Chem. Phys.*, **88**, 3976 (1988).
[18] D. Stauffer, "Introduction to percolation theory", Taylor & Francis, 1987.
[19] M. Adam and M. Delsanti, "Percolation-type growth of branched polymers near gelation", *Contemporary Physics*, **30**, 203 (1989).
[20] D. Adolf and J.E. Martin, "Dynamic properties of sol-gels", in *Fractal Aspects of Materials-1989*, ed., J.H. Kaufman, J.E. Martin and P.W. Schmidt (MRS, Pittsburgh, 1989).
[21] D.M. Heyes, "Transport coefficients of Lennard-Jones fluids: a molecular-dynamics and effective-hard sphere treatment", *Phys. Rev. B*, **37**, 5677 (1987).
[22] K.D. Hammonds and D.M. Heyes, "Transport coefficients of model simple liquids: a molecular-dynamics study and effective hard-sphere analysis", *J. Chem. Soc., Faraday Trans. 2*, **84**, 705 (1988).
[23] D.M. Heyes and J.R. Melrose, "Microscopic simulation of rheology: molecular dynamics computations and percolation theory", *Mol. Sim.*, **2**, 281 (1989).